The following publication Chang Guo, Chao Zhou; Axial behaviour of steel pipelines buried in sand: effects of surface roughness and hardness. Geotechnique 1 June 2025; 75 (6): 800–813 is published by Emerald and is available at https://doi.org/10.1680/jgeot.24.00001.

Axial behaviour of steel pipelines buried in sand: effects of surface roughness and hardness

Authors: Chang Guo and Chao Zhou*

*Corresponding author

Information of the authors

First author: Mr Chang Guo

PhD student, Department of Civil and Environmental Engineering, The Hong Kong Polytechnic University, Hung Hom, Hong Kong. E-mail: chang.guo@connect.polyu.hk

Corresponding author: Dr Chao Zhou

Tsui Tack Kong Young Scholar in Civil Engineering, Associate Professor, Department of Civil and Environmental Engineering; Research Institute for Sustainable Urban Development, The Hong Kong Polytechnic University, Hung Hom, Hong Kong. E-mail: c.zhou@polyu.edu.hk

ABSTRACT

Surface roughness and coating hardness of underground pipelines are expected to play decisive roles in their axial pullout behaviour, which is an important aspect of pipeline design. Existing guidelines and previous studies underestimated or ignored these effects, resulting in potentially unsafe design. To address this problem, the current study conducted nine large-scale physical modelling tests on pipes in dry and dense sand. Five steel pipes with varying normalised roughness (0.04-1.01) and coating hardness (32.6-59.0 HRA) were used and instrumented with a novel type of film-like piezoresistive sensors for measuring soil-pipe contact pressure. The measured pullout resistance of rough pipes is 2.70-2.85 times of smooth pipes, significantly greater than the value specified in current design guidelines (i.e., 1.17 times). This substantial increase stems from an increase in interface friction coefficient (accounting for 72-79%) and a contact pressure increase induced by constrained dilation and soil arching (contributing the remaining 21-28%). Regarding coating hardness, a critical hardness was observed (around 35 HRA). Due to equivalent roughness from particle embedding, pipes with hardness below this value exhibited similar behaviour to rough pipes. Finally, a new and simple method was proposed for calculating the pullout resistance with consideration of the effects of roughness and dilatancy.

Keywords

Pipes & pipelines; Buried structures; Model tests; Soil/structure interaction

Introduction

In pipeline engineering, surface treatment techniques such as coating, wrapping, and sand-blasting are commonly employed on underground pipelines to prevent corrosion, adjust resistance and provide thermal insulation (ISO 8501-1, 2007; CEDD, 2020). These treatments can greatly impact the pipe surface roughness and hardness, which are expected to affect the soil-pipeline interaction that may happen during landslides, earthquakes, and thermal expansion/contraction. So far, some researchers have investigated the influence of surface roughness and hardness on soil-pipe interaction in the lateral and vertical directions. Physical model tests by Trautmann & O'Rourke (1985) and Trautmann et al. (1985) have demonstrated that variations in lateral resistance and uplift vertical resistance for pipes with different surface roughness and coating materials are approximately 10% and 10-30%, respectively. These results suggest that the impact of surface roughness and hardness on the lateral and vertical interaction is not substantial, as they are primarily governed by the surrounding soil behaviour. In contrast, the behaviour of axial soil-pipeline interaction (ASPI) is likely influenced by the interface characteristics between the soil and pipe. Consequently, roughness and hardness, which significantly affect interface shear strength and dilatancy, are crucial determinants of axial resistance, as indicated by research from Dove & Frost (1999), Han et al. (2018) and Ghanadizadeh et al. (2022). Neglecting their influences on the axial load evolution may lead to unsafe or uneconomical designs of pipeline systems (O'Rourke et al., 1990; Klar & Marshall, 2008). For instance, underestimating the axial force imposed by potentially moving soils could lead to unsafe pipeline design.

As a widely used design guideline, ASCE (1984) calculates the pullout resistance (i.e., the maximum axial force per meter length) of pipes buried in sands, T_{max}, using the Mohr-Coulomb theory. It is assumed that the average contact pressure (namely, the average normal stress) on pipes is equal to the mean of nominal vertical pressure at the pipe crown, σ_c' (= $\gamma' H_c$), and its lateral earth pressure at rest $K_0 \sigma_c'$. Hence, T_{max} can be calculated as follows:

$$T_{\max} = \pi D \frac{1+K_0}{2} \sigma_c' \tan\delta \tag{1}$$

where D is the pipe outer diameter; γ' is the effective unit weight of the backfill sand; H_c is the buried depth of the pipe crown; $\tan\delta$ is the soil-interface friction coefficient; δ is the interface friction angle. ALA (2001) and PRCI (2009) further specify that $\delta = f\varphi'$, where f is the soil-pipe interface friction factor and φ' is the internal friction angle of sand. The value of f is recommended based on the surface roughness and coating materials (related to surface hardness), as summarised in Table 1. The classification of surface conditions is qualitative but not quantitative. More importantly, this equation only considers the roughness and hardness effects on δ but ignores their impacts on the contact pressure between soil and pipe during ASPI (Lings & Dietz, 2005; Abuel-Naga et al., 2018). The evolution of contact pressure could be complex due to various factors, especially the constrained dilatancy and soil arching. For instance, Wijewickreme et al. (2009) conducted three physical modelling tests in dense soil with one rough steel pipe. The experimental results and corresponding numerical simulations show that the constrained dilation increased the contact pressure on the pipe surface and, thus, the pullout resistance. In addition, constrained dilatancy may interact with other factors, such as soil stiffness and pipe diameter (Yin et al., 2012; Wijewickreme & Weerasekara, 2015). Sheil et al. (2018) tested one heavy steel pipe coated by fusion-bonded epoxy (FBE). The soil arching was found to affect the contact pressure and the pipe pullout behaviour.

As far as the authors are aware, no physical model test has been reported in the literature for investigating the effects of surface roughness on ASPI. Regarding the effects of coating on the pullout behaviour of pipelines, only Scarpelli et al. (2003) conducted three valuable but simple field tests using sands with steel pipes coated by polyethene and coal tar. The pullout resistances of pipes with harder surfaces were smaller than those of softer pipes. The role of soil arching and constrained dilatancy was not explored. Clearly, more experimental results are needed to understand and quantify the effects of roughness and hardness on the ASPI mechanism and pullout resistance.

In this research, a large-scale experimental system was developed to study ASPI. Nine pullout tests were conducted using five pipes with different surface treatments, including three surface roughness and two coating materials. The main objectives are: (a) to investigate the extent to which surface roughness and hardness affect the pullout resistance, (b) to examine the mechanisms of surface condition effects, and (c) to propose a new method of calculating pipe pullout resistance.

A new and large-scale experimental system

An experimental apparatus for testing ASPI was modified from the soil nail testing system of Yin & Su (2006), as shown in Fig. 1. It consists of a steel box, pipes, an axial actuation subsystem, and a vertical loading subsystem. The steel box with strengthening beams was used to simulate the pipeline trench conditions. It has internal dimensions of 1.0 m in length, 0.8 m in height, and 0.6 m in width. This width meets the minimum requirements of the trench for pipes with a diameter of less than 150 mm, as specified in the guideline of USBR (1996). Two holes are provided on the front and rear walls. The pipe can pass through these holes to ensure a constant soil-pipe interaction length during the pullout process.

The front and rear walls of the box would cause non-uniform shear stress distribution along the pipe. This problem was observed in physical model tests by Al-Khazaali & Vanapalli (2019) and DEM simulation by Meidani et al. (2017). Therefore, this study introduced two pipe sleeves with an inner diameter of 132 mm to avoid the soil-pipe interaction in the zone close to the front and rear walls. Their efficiency in minimizing boundary effects is discussed later. The sleeves inside the box are 0.15 m long, resulting in a soil-pipe interaction length of 0.7 m.

The axial actuation subsystem, including an electric linear actuator, a servo control panel, and a reaction frame, was used to impose axial displacement. A connector (see Fig. 1) was introduced to allow a free relative vertical movement between the pipe and the actuator. Rubber sleeve membranes with a nominal inner diameter of 100 mm and a nominal thickness of 1.5 mm were inserted between the pipe and sleeves to prevent soil leakage. The pipe and sleeves were aligned coaxially, creating a gap of approximately 8.5 mm (22 d_{50} of the sand used in this study) between the pipe and sleeves. This gap provides sufficient space for pipe settlement (no more than 0.5 mm in this study) and the development of interface shear zone (2-10 d_{50}, DeJong & Westgate (2009)).

A flexible pneumatic bag (see Fig. 1) was installed between the soil and the top cap. The length and width of the pneumatic bag match the dimensions of the box's interior. By adjusting the air pressure P inside the bag, the nominal pressure at the crown, σ_c', can be controlled by $\sigma_c' = \gamma' H_{c0} + P$, where H_{c0} = real buried depth from the ground surface to the crown of the pipe.

Pipes with different surface roughness and hardness

Hot-rolled seamless steel pipes, commonly used in Hong Kong, with a nominal outer diameter of 102 mm and a nominal thickness of 4 mm, were used (BSI EN 10220:2002, 2002; HKIUS, 2011). Further details can be found in Table 2. The effects of fluid weight on the pipe pullout mechanism might be insignificant in most cases, and they are not considered here. Smooth, intermediate, and rough pipes were prepared using three non-coated raw steel. Their surface roughness was quantified with the normalised surface roughness (R_n) using the equation by Kishida & Uesugi (1987): $R_n = R_{max}/d_{50}$, where d_{50} is the average particle size, and R_{max} is the maximum height on the surface profile over a travel length of d_{50}. It should be noted that different classification methods for rough, intermediate and smooth pipes are available in the literature. One method is based on the variation of interface friction angles with the normalised roughness. The interface friction angles increase with the normalised roughness for intermediate interfaces and normally keep constant for smooth and rough interfaces. The critical values of normalised roughness that differentiate smooth-intermediate and intermediate-rough interfaces are 0.02 and 0.5, respectively, as suggested by Paikowsky et al. (1995). Alternatively, some researchers use dilation/contraction during shearing (Lings & Dietz, 2005; Farhadi & Lashkari, 2017): the critical value of normalised roughness transiting the intermediate to rough ranges is normally 0.1-0.2 in this framework. The first approach is adopted in the current study. Without any treatment, the raw seamless steel pipe has a roughness value of 0.04, as measured by a surface roughness tester (SJ-210, Mitutoyo). Although slightly larger, this value is very close to the critical value of 0.02, so the raw pipe is referred to as a smooth pipe in this study. The surfaces of the rough and intermediate pipes were treated using the turning method. Turning depths of 0.38 mm with an interval of 0.9 and 0.08 mm with an interval of 0.4 mm were applied to achieve normalised roughness values of 1.01 and 0.21, respectively.

Two commonly used coatings, epoxy asphalt (EA) and fusion bonded epoxy (FBE), coated two raw steel pipes to evaluate the hardness effects. Surface hardness tests were conducted using the Rockwell hardness scale of HRA by a hardness tester (OMAG 206) (ASTM E18, 2022; ASTM D785, 2023). The measured hardness values for EA, FBE, and raw steel are 32.6, 44.2, and 59.0, respectively. The measured values of R_n of the two coated pipes are both 0.01.

Instrumentation

A novel Force Sensing Resistor (FSR), namely FSR 402 from Interlink Electronics, was used to measure earth pressure and soil-pipe contact pressure (Interlink, 2023). It is a piezoresistive sensor whose electric resistance is a function of pressure. Its thinness and flexibility can effectively eliminate the arching effects on sensors and conform well to curved surfaces (Liu et al., 2021; Kootahi & Leung, 2022). To measure earth pressure (Application I in this study), each FSR was affixed to a 1 mm-thick steel slice and coated with epoxy adhesive, as shown in Fig. 2. Five FSRs for Application I were utilised to measure the vertical soil stress at various depths, as depicted in the side view of Fig. 1. As for measuring the soil-pipe contact pressures (Application II), FSRs were installed on the pipe surface (see Figs. 1 and 2). To facilitate wire routing, small holes were created in the pipe, and the sensors were secured and protected using epoxy adhesive while the holes were sealed. Eighteen FSRs were deployed across three cross-sections with a spacing of 0.2 m between sections. Each cross-section included six FSR sensors mounted at the crown, one shoulder, two springlines, one haunch, and the invert (see Fig. 1).

FSR's electrical conductance (the reciprocal of electrical resistance) was measured using a datalogger of dataTaker DT85G. The pressure-conductance relationship is found to be dependent on the specific installation condition of each sensor, so post-installation calibration is necessary. The sensors in Application I were put into a sealed tank. As for Application II, pipe repair clamps, consisting of a rubber sleeve with thickened edges and a steel split sleeve with screws, were used to form a sealed space for the sensors. A hole was punched in the middle of the repair clamp and connected hermetically to a pneumatic connector. By adjusting the air pressure in the sealed tank/space, the relationship between pressure and output can be determined. A typical pressure-conductance relationship with a loading rate of 4 kPa/min from 0 to 200 kPa is shown in Fig. 2. The mean of non-linearity error within a measurement range of 0-200 kPa from calibration results of eighteen FSR sensors is approximately 5.8%. To improve the accuracy, a nonlinear signal processing method was employed: the calibration results were fitted using the smoothing spline algorithm in MATLAB (see the line in Fig. 2). In addition, the influence of shear stress on the FSR reading was assessed through two direct shear tests. One FSR sensor was installed on a steel interface with an R_n of 1.01. Under effective normal pressures of 55 and 110 kPa, the shear stresses were increased from 0 to the interface strengths of 47 and 73 kPa, respectively. During shearing, the differences between the measured and applied effective normal pressures were all below 10%.

An optic fibre was utilised for the optical frequency domain reflectometry (OFDR) method to measure the pipe axial strain distribution to verify the feasibility of sleeves and rubber membranes. This fibre was attached to the pipe's inner surface at two shoulders and two haunches.

Two linear variable differential transformers (LVDTs) were utilised to measure the pipe's vertical displacement. Additionally, a load cell with a measurement range of ± 10,000 N and an LVDT with a measurement range of 50 mm were adopted to monitor the axial force and axial displacement, respectively. The locations of these sensors are shown in Fig. 1.

Test materials

The testing soil is standard medium sand sourced from Fujian Province, China, with a particle size ranging from 0.25 to 0.5 mm. Its properties are summarized in Table 2. The target relative density is 85%. A series of direct shear tests were conducted to measure the internal friction angle of pure sand and the interface friction angle between sand and interfaces (treated using the same methods on pipes). The shear box and test method are similar to those of Cui et al. (2024). The sizes of specimens in direct shear tests and interface direct shear tests were 60 × 60 × 40 mm and 60 × 60 × 20 mm, respectively. The shear rate was 0.02 mm/s, consistent with the pipe pullout speed in the following physical modelling. The effective normal stresses were set as 17, 34, 50, and 100 kPa, corresponding to the target nominal pressure at the pipe crown in the physical modelling. The results are shown in Table 3.

Testing programme

Two series of pullout tests were conducted, as summarised in Table 4. Series I consisted of seven tests to study the effects of roughness and stress. Smooth and rough pipes were buried at different nominal pressures σ_c'. The target nominal pressures σ_c' include 17, 34, and 50 kPa, corresponding to 1, 2, and 3 m in burial depths. An intermediate pipe was also tested under a nominal pressure σ_c' of 34 kPa. Series II involved the pullout testing of FBE-coated and EA-coated pipes under a nominal pressure σ_c' of 34 kPa. These coated pipes were compared with the smooth pipe to analyse the effects of coating hardness.

Model preparation and test procedures

The sand pluviation method (Fretti et al., 1995) was introduced to prepare dense and uniform samples and simulate the dumping technique in the engineering practice of compaction. The models were prepared in layers. Each layer had a thickness of approximately 25 mm. A laser level magnetically attached to the box's inner wall and six rulers affixed to the side walls were used to get a flat surface for each layer. During preparing the sample, sleeves were installed once the depth reached 0.28 m. At an elevation of 0.33 m, the pipe with rubber membranes was put into the box. The soil around the ends of the sleeves was temporarily moved, and after placing the rubber membranes and adjusting the pipe to the desired position, the removed soil was backfilled and compacted to its original state using a square wooden mallet. At this stage, the pipe was buried to a depth equalling 30% of its diameter. Subsequently, sand was continuously added until the elevation reached 0.76 m.

After preparing the sample, the pneumatic bag and top cap were put on the soil. The air pressure was controlled, and this condition was maintained for approximately 30 minutes until sensor readings, such as vertical displacement and earth pressure, stabilised. Finally, the pullout speed of the pipe was set as 0.02 mm/s, and the target displacement was 20 mm, both of which are common values in previous studies (Sheil et al., 2018; Reza & Dhar, 2021).

Evaluation of boundary effects

Two boundary effects were addressed in this study. The first one is the non-uniform distribution of shear stress caused by the presence of front and rear walls. As mentioned above, two sleeves with rubber membranes were introduced to address this problem. Fig. 3 illustrates the axial strain distribution measured by optic fibre with various axial displacements using the rough pipe under a surcharge of 50 kPa. The square points represent the axial strain at the side of the actuator (d = 700 mm) calculated by the axial force measured by the load cell, Young's modulus of steel and pipe cross-sectional area. These measurements align with the micro strains obtained through the fibre at the pipe end, confirming the accuracy of the strain measurement. Throughout the pullout process, the distance *d* and the axial strain show a good linear relationship (R-squared > 0.99). It indicates that the non-uniformity of the shear stress distribution was minimised successfully by sleeves and membranes and that the size of the gap between pipe and sleeves is applicable to guarantee sufficient lateral support for the surrounding soils by rubber membranes.

The second boundary effect pertains to the roughness of the side walls. Two tests were conducted using the smooth pipe under a surcharge of 34 kPa. The side walls of the first test consisted of smooth steel plates (R_n = 0.01), while for the second test, two pieces of sandpaper with a grit size of P40 ($R_n \approx 1.13$) were attached to the steel plates to simulate rough trench conditions. The measured axial resistance-displacement relationships for the two tests exhibit remarkable consistency, suggesting that the roughness of the side walls has negligible effects.

Experimental results and discussion

Roughness effects on pullout force-displacement relationship and pullout resistance

Fig. 4 illustrates the relationship between axial displacement and mobilised axial resistance in Series I. The axial pullout behaviour is significantly influenced by roughness. The results show that rough and intermediate pipes exhibit obvious strain-softening behaviour, while strain-softening is negligible for smooth pipes. This finding aligns with the results of soil-interface direct shear tests, where rough interfaces exhibit significant dilatant behaviour, while smooth interfaces show limited dilation. Under the same nominal pressure, the pullout resistance of rough pipes is 1.70-1.85 times higher than smooth pipes. This value is much larger than 0.17 ($\tan(0.8\varphi')/\tan(0.7\varphi')$-1) suggested by guidelines (see Table 1). Such a significant increment is due to different mechanisms. The increase in friction coefficient from soil-pipe smooth to rough soil-pipe interfaces (see Table 3) is 1.34 times ($\tan(37.9°)/\tan(18.4°)$-1). It means that

72-79% of the roughness-caused resistance increase is attributed to the increase in interface friction coefficient. The remaining 21-28% is mainly attributed to the increment of soil-pipe contact pressure that is closely related to the constrained dilation, as discussed later.

Fig. 5 demonstrates the relationship between the pullout resistance and the nominal vertical pressure at the crown for rough and smooth pipes. For both pipe types, the intercept of the trend line is higher than zero if assuming a linear envelope. This phenomenon is similar to the nonlinear failure envelope in interface shear. The soil's dilatancy becomes more pronounced at lower pressure, leading to this non-linearity.

Fig. 6 (a) compares the interface friction coefficients measured in the interface direct shear tests (μ_{dir}) (see Table 2) and predicted by the guidelines (μ_{ALA}) (see Table 1) to μ_{phy} (= $T_{\mathrm{max}}/[\pi D(1/2)(1+K_0)\sigma_c']$). The value of μ_{dir} ranges from 0.49 to 0.78, aligning with the findings of previous shear studies on dense sand-structure interfaces (Lings & Dietz, 2005; Farhadi & Lashkari, 2017; Han et al., 2018). μ_{ALA} is calculated from tan$f\varphi'$. The guidelines (ALA, 2001; PRCI, 2009) do not define "rough" and "smooth"; thus, a range is depicted in Fig. 6 (a). According to Table 1, the values of μ_{ALA} for smooth and rough steel pipe are tan$0.7\varphi'$ (= 0.53) and tan$0.8\varphi'$ (= 0.62), respectively. Finally, μ_{phy} is the back-calculated value based on pullout resistances from physical modelling and Eq (1), representing the ratio of the pullout resistance to the assumed soil-pipe contact force per unit length. For the sake of simplicity in expression, it is denoted as μ_{phy}, although it differs from the concept of the interface friction coefficient given changes in soil-pipe contact pressure during the pullout process. The value of μ_{phy} ranges from 0.45 to 1.52 and increases with the normalised roughness, showing an approximate linear relationship with the logarithmic value of roughness. If the average contact pressure is constant (CNL conditions) during pullout, μ_{phy} should be equal to μ_{dir}. However, μ_{dir} consistently remains lower than μ_{phy} in Fig. 6 (a). It implies that the average contact pressure on the pipe surface increased during the pullout process. The pipe pullout behaviour aligns more closely with the constant normal stiffness (CNS) condition rather than the CNL condition due to the constrained dilation behaviour (DeJong & Westgate, 2009; Pra-ai & Boulon, 2016; Ng et al., 2020; Zhou et al., 2020): the presence of sands far away from the interface constrains the dilation trend at the interface, leading to an increase in contact pressures during shearing. The dilatancy of the soil-pipe interface is positively correlated with the interface roughness (Lings & Dietz, 2005; Zhang et al., 2011; Farhadi & Lashkari, 2017). Therefore, although μ_{dir} also increases as the roughness increases, its growth rate with roughness increase is not as steep as that of μ_{phy} and their difference, μ_{phy}-μ_{dir}, widens with increasing roughness.

The values of μ_{ALA} only encompass a small range of the measured values of μ_{phy}. The guidelines slightly overestimate smooth pipes' pullout resistance and significantly underestimate that of rough pipes. Both underestimation and overestimation can pose safety risks to the pipeline system. Underestimation implies a lower design pipeline strength. When there is any relative axial displacement between the pipe and the soil, the stress experienced by the pipe may exceed the pipeline strength, potentially causing damage to the pipe. On the other hand, overestimating the pullout resistance results in higher expectations for the soil's ability to limit deformation in the pipeline system. This can potentially lead to issues like upheaval buckling due to thermal expansion, bending due to nearby tunnel construction (Marshall et al., 2010; Wang et al., 2011), or excessive loads concentrated on weak points, such as valve stations or cracks in the piping system, as discussed by PRCI (2009). Moreover, the wide range of μ_{phy} underscores the importance of quantifying roughness in pipeline design rather than relying on the qualitative definition provided by guidelines (ALA, 2001; PRCI, 2009).

Roughness effects on contact pressures distribution and evolution

Fig. 7 illustrates the distribution and evolution of contact pressures for smooth and rough pipes subjected to a nominal vertical pressure of 34 kPa at the crown. The difference in the contact pressures measured by FSR sensors is generally within ±10% of the average value at the corresponding positions on the three cross-sections. The contact pressure difference between the left and right springlines is kept under 2 kPa, indicating good symmetry. Therefore, the average values at the crown, shoulders, springlines, haunches, and invert are directly displayed. The contact pressure assumed by the guidelines is σ_c' (34 kPa) at the crown and invert, $K_0\sigma_c'$ (12.3 kPa, K_0 takes as 1- sin φ') at the springlines, $(1+K_0)\sigma_c'/2$ (23.2 kPa) at the shoulders and haunches, respectively.

Before the pullout, the roughness did not affect the initial contact pressure distribution. It is distributed with the shape of a "Norman Shield", as shown in Fig. 7. This shape is consistent with the testing results of Wijewickreme et al. (2009) and Sheil et al. (2018). The contact pressures at the invert and shoulders are always larger than the assumed values, while those at the crown, springlines, and haunches are normally less than the expected value. However, the differences between measured values and expected values are typically not more than 25% of expected values. The mean values of initial average contact pressure with σ_c' of 17, 34, and 50 kPa are 12.6, 22.5, and 37.5 kPa, respectively. These average values closely align with the assumed values by $(1+K_0)\sigma_c'/2$ (11.6, 23.2, and 34.1, respectively) because the increase and decrease in contact pressure at different locations offset each other. Calculating the initial average contact pressure using $(1+K_0)\sigma_c'/2$ is acceptable.

During the pullout process, the contact pressures on different pipes exhibit an overall increasing trend, with the magnitude of the increase being positively correlated with the roughness (see Fig. 7). This finding supports the explanation provided earlier regarding why μ_{phy} consistently exceeds μ_{dir} and why μ_{phy}-μ_{dir} is influenced by the roughness and hardness of the pipe surface.

Different evolution processes of contact pressures reflect on pipes with different roughness. For the rough pipe (Fig. 7 (b)), the contact pressure increase is persistent and notable. This increase predominantly occurs at the crown and the invert, where the pressures can reach around 55 and 70 kPa, respectively. The increase at the springlines (around 8 kPa) is insignificant. Moving to the smooth pipe (Fig. 7 (a)), most of the contact pressures experience an initial increase before reaching a displacement of 3 mm, a subsequent decrease after the peak, and finally, a slight increase. This fluctuation trend is similar to the results of Wijewickreme et al. (2009).

Effects of soil arching and constrained dilatancy on pipe pullout mechanism

The distribution and evolution of soil-pipe contact pressure in Fig. 7 are closely related to the soil arching effects (Sheil et al., 2018; Meguid, 2019), and they are explained using the schematic diagram in Fig. 8. During the backfilling process, the soil above the pipe is expected to experience a smaller settlement than the soil at the pipe sides, owing to the stiffening effects of pipe. The relative movement results in internal friction in the soil, concentrating more pressure on the pipe, especially at the crown, shoulders and the invert. This pressure concentration also causes the pipe to settle. In this study, the measured pipe settlements during this process are 0.1-0.5 mm, increasing pressure at the invert but reducing the pressure at the crown towards σ_c'. In addition, the concentration of overburden pressure on the pipe reduces the vertical pressure on the sides, thus lowering the contact pressure on the springlines (lateral earth pressure).

During the pullout process, the evolution of soil-pipe contract pressure is likely affected by two different mechanisms. Firstly, shearing at the soil-pipe interface disturbs the original stress equilibrium, weakening the soil arching effects developed during the backfilling process and tending to reduce the contact pressure. Secondly, the constrained dilation at the soil-pipe interface tends to increase the contact pressure and could cause additional soil arching due to further relative vertical displacement between the soils at pipe sides and above the pipe, resulting in a more significant increase of contact pressures at the crown, shoulders, and invert. The overall change in contact pressure depends on the relative importance of these mechanisms.

For the smooth pipe, the contact pressure at most points increases slightly due to the second mechanism, while contact pressure at the springlines increases more significantly due to the first mechanism, as shown in Fig. 7 (a). As for the rough pipe, the second mechanism likely plays a dominant role (Martinez & Frost, 2017). The average contact pressure increases sharply due to its significantly constrained interface dilation behaviour. The additional soil arching makes this increase concentrate on the crown and invert and the vertical component of the contact pressures of shoulders and haunches. This additional soil arching also weakens the overburden vertical pressure on the soil of the pipe sides, reducing the corresponding lateral earth pressure (contact pressure at the springlines). It offsets part of the contact pressure increase caused by constrained dilation, resulting in limited pressure change at the springlines (as shown in Fig. 7 (b)).

The evolution of earth pressure in Fig. 9 further supports the above explanation. Before pullout, the earth pressures above and below the pipe are consistently greater than the earth pressure on the pipe sides with the same level due to the pressure concentration on the pipe. During the pullout process, the earth pressures around the smooth pipe remain unchanged or increase slightly, indicating that the impact of dilation behaviour is limited. In contrast, the earth pressures above and below the rough pipe experience significant growth, while the vertical pressure on the pipe sides slightly decreases. This is consistent with the evolution of contact pressures shown in Fig. 7 (b).

Roughness effects on stress path

Fig. 10 illustrates the stress paths at the soil-pipe interfaces in physical modelling. The failure envelopes of three interfaces are determined through CNL interface direct shear tests and included as references. The shape of the stress path remains unaffected by the overburden pressure but is influenced by the roughness. For the smooth pipe, the stress path generally includes four stages. In the first stage, the stress path rises vertically, meaning the friction angle mobilisation is essentially elastic during this process. Then, the path turns to the second stage by moving towards the top right direction. It illustrates an increase in average contact pressure caused by constrained dilatancy, as explained above. Subsequently, the stress path turns to the upper left in the third stage due to the average contact pressure decrease caused by the disturbance of soil arching. During the ultimate stage, the path moves slightly to the bottom right after touching the peak failure envelope. It indicates a slow decrease in the mobilised friction angle and slight constrained dilation behaviour.

As for the stress paths of rough and intermediate pipes, they generally include three stages resembling the typical stress path observed in constant normal stiffness (CNS) tests on the rough interface (Ooi & Carter, 1987; Pra-ai & Boulon, 2016). The stress paths of rough and intermediate pipes during the first and second stages are similar to those of smooth pipes, which rise vertically and then turn to the top right. The major difference is that, before touching the peak failure envelope, the stress path keeps the trend moving towards the top left rather than undergoing the smooth pipes' third stage due to its significant constrained dilation. Subsequently, the stress paths turn to the bottom right and tend to touch the critical state envelope in the third stage of rough and intermediate pipes. During this process, the degradation of the mobilised friction angle is much more evident than the further increase in contact pressure, corresponding to the obvious softening behaviour in Fig. 4.

Coating hardness effect on pullout behaviour

Moving on to the coating hardness effects in Series II, the pullout force-displacement curves of the EA-coated and FBE-coated pipes in Fig. 4 resemble those of rough and smooth pipes, respectively, although the values of normalised roughness are both small for these two coated surfaces. Additionally, the resistance of the EA-coated and FBE-coated pipes is close to that of rough and smooth pipes, respectively (see Fig. 5). These observations are mainly related to particle embedment. After tests, numerous particles were found embedded in the surface of the

EA-coated pipe, while no embedment or scratches were observed on the FBE-coated pipe (see Series II in Fig. 4). The pipes coated with softer materials may be considered a specialised form of rough pipe due to the increase in equivalent roughness caused by embedment. Conversely, the pipes coated with harder materials do not experience this increase in equivalent roughness.

The above results are further supported by Fig. 6 (b). On the one hand, μ_{phy} for EA-coated, FBE-coated, and smooth steel pipes are 1.21, 0.45, and 0.45-0.54, respectively, larger than the corresponding μ_{dir} values of 0.75, 0.35, and 0.33. The μ_{phy}-μ_{dir} of EA-coated and FBE-coated pipes also closely resemble those of rough and smooth pipes, respectively. On the other hand, similar to rough pipes, the resistance of pipes with soft material coatings (such as coal tar and EA) is notably underestimated by the guidelines, as shown in Fig. 6 (b). This underestimation can be attributed to the dilation behaviour. Additionally, μ_{phy} for EA-coated is slightly smaller than that of the rough steel pipe. The reason might be that the stiffness of the coating layer is much smaller than steel. A volume change in the coating layer would happen, though not large, due to the limited coating thickness, reducing the contact pressure increase caused by constrained dilation. Hence, the axial resistance of the EA-coated pipe is slightly lower. However, μ_{phy} of FBE-coated pipe aligns well with the guidelines' predictions because there is limited dilatancy at the hard and smooth interface, making its axial pullout behaviour resemble the assumption of the guidelines.

There appears to be a critical hardness of around 35 HRA. The resistance of pipes with hardness less than this critical value is susceptible to surface hardness, whereas, for pipes with surface hardness greater than this value, the effect of hardness on ASPI is minimal. This concept of critical hardness has also been used by Abuel-Naga et al. (2018). It is highlighted that the above value of critical hardness cannot be generalised because it is also dependent on other important factors, such as normal pressure, particle angularity, size, and grain size distribution based on the experimental results on soil-geomembranes by Frost & Han (1999) and Dove & Frost (1999). Particles overall morphology of this sand measured by Liang et al. (2021) is given in Table 2 for information.

Development of a new method for calculating pipe pullout resistance

Fig. 11 compares the measured values of pullout resistance with the ALA predictions (Eq. (1)) using the experimental results in Wijewickreme et al. (2009), Sheil et al. (2018), and this study. The interface friction angle, δ, uses the value measured by direct shear testing. Eq. (1) cannot predict the axial resistance well, especially for rough pipes buried in dense sands. As discussed earlier, this equation neglects the contact pressure increase caused by constrained dilation. Additionally, it does not account for the effects of pipe self-weight, as Sheil et al. (2018) highlighted. A new equation is proposed to address these limitations as

$$T_{\max} = \left[\pi D(\gamma' H_{\mathrm{c}} \frac{1+K_0}{2} + \Delta\sigma_{\mathrm{D}}') + \Delta W\right] \tan\left(f_R \varphi'\right) \tag{2}$$

where three new terms are introduced: $\Delta\sigma_{\mathrm{D}}'$ is the average increase in contact pressure caused by constrained dilation; ΔW is the normal force increase per unit length caused by the pipe weight; and f_{R} is the roughness-dependent soil-pipe interface friction factor. The determination of these three terms is explained below:

Firstly, $\Delta\sigma_{\mathrm{D}}'$ can be determined by the linear elastic expanding cylinder theory, as given by Houlsby & Italiana (1991):

$$\Delta\sigma_{\mathrm{D}}' = 4G\frac{u_{\mathrm{r}}}{D} \tag{3}$$

where u_{r} is the radial expanding displacement of the shear band due to interface dilation and G is the soil shear modulus. This model was further developed to predict the pullout resistance of soil nails and pipes in subsequent studies (Luo et al., 2000; Yin et al., 2012; Wijewickreme & Weerasekara, 2015). u_{r} can be determined as follows:

$$u_{\mathrm{r}} = \int_0^{u_{\mathrm{c}}} \frac{du_r}{du}\mathrm{d}u = \int_0^{u_{\mathrm{c}}} \frac{du_r/S}{du/S}du = \int_0^{u_{\mathrm{c}}} \frac{d\varepsilon_v}{d\gamma}du = \int_0^{u_{\mathrm{c}}} \tan\psi du \tag{4}$$

where u_c is the critical axial displacement where the mobilised dilation angle reaches its peak value; S is the thickness of the shear band; $d\varepsilon_v$ is the volumetric strain increment, equaling du_r/S for the soil in the shear band; $d\gamma$ is the shear strain increment, equaling du/S; tan ψ (= $d\varepsilon_v/d\gamma$) is the dilatancy. Luo et al. (2000) and Yin et al. (2012) assumed that tanψ linearly increases with the axial displacement until reaching the maximum dilation angle (ψ_{max}). Under this assumption, u_r can be further calculated by

$$u_\mathrm{r} = \int_0^{u_\mathrm{c}} \tan\psi \mathrm{d}u = \int_0^{u_\mathrm{c}} \frac{u}{u_\mathrm{c}} \tan\psi_\mathrm{max} du = \frac{1}{2} u_\mathrm{c} \tan\psi_\mathrm{max} \tag{5}$$

Assuming that the mobilised dilation angle and the mobilised pullout resistance reach their peak values at the same critical axial displacement u_c, Eqs. (3) and (5) suggest that

$$\Delta\sigma_\mathrm{D}' = 2G \frac{u_\mathrm{c}}{D} \tan\psi_\mathrm{max} \tag{6}$$

where u_c is affected by surface roughness and coating hardness. The method of Audibert & Nyman (1977) is employed to determine u_c from the results in Fig. 4. This method consists of a horizontal line through the maximum resistance and a secant line passing through the origin and the point of 70% of the maximum pullout resistance. The intersection of these two lines determines u_c. Table 5 summarises the values of u_c for different pipes in this study and Wijewickreme et al. (2009). u_c for non-coated steel pipes ranges from 0.77 to 2.85 mm, showing a positive correlation with the normalised roughness. u_c for FBE-coated and EA-coated pipes are 1.85 and 3.76 mm, relatively larger than those of the non-coated steel pipes.

On the other hand, ψ_{max} in Eq. (6) can be determined using the method of Bolton (1986), which can be simplified as

$$\psi_\mathrm{max} = A_\psi / a_\psi \left[I_\mathrm{D}(Q - \ln\sigma_f') - R \right] \tag{7}$$

where I_D is relative density; σ_f' is the effective stress at failure; a_ψ, A_ψ, Q and R are empirical coefficients. For dense sand at low pressure ($I_D(Q$-ln$\sigma_f')$-R>4, common in soil-pipe interaction), Chakraborty & Salgado (2010) obtained values of these four coefficients as 0.62, 3.8, 7.1 +

0.75ln σ_i', and 1, respectively. σ_i' is the initial effective stress, taken as $\gamma' H_c(1+K_0)/2$ in this study. It should be noted that σ_f' is the effective normal stress at the failure, but it is hard to determine the effective stress at failure σ_f' in Eq. (7) for engineers. Hence, σ_f' is also approximately taken as the average initial effective stress, $\gamma' H_c(1+K_0)/2$, in this study. The potential error of this approximation on ψ_{max} is as small as not more than 4% based on the value of Q and R.

Moreover, G can be determined by the model of Oztoprak & Bolton (2013) as

$$G = \frac{A(\gamma)\cdot p_a}{(1+e)^3}\cdot\left(\frac{\sigma_i'}{p_a}\right)^{m(\gamma)} \tag{8}$$

where e is the void ratio; p_a is a reference pressure of 100 kPa. $A(\gamma)$ and $m(\gamma)$ are empirical parameters dependent on the shear strain γ (= u/S). Based on the values of u_c in Table 5 and the empirical data in interface shear band thickness (DeJong & Westgate, 2009), the critical interface shear strains at which the mobilised pullout resistance reaches their peak values are determined to be no less than 10%. It is practical to adopt the empirical values of $A(\gamma)$ = 126 and $m(\gamma)$ = 1 for γ =10%, as suggested by Oztoprak & Bolton (2013).

Secondly, ΔW can be calculated by the product of the pipe's volume per meter V and the unit weight difference ($\Delta\gamma$) between the pipe and backfilled soil as

$$\Delta W = V\Delta\gamma = \frac{\pi D^2}{4}\left(\bar{\gamma}_{pipe} - \gamma_b\right) \tag{9}$$

In this equation, $\bar{\gamma}_{pipe}$ is the apparent unit weight of the pipe. It is the ratio between the actual pipe weight (the total weight of pipe and fluid contained in the pipe under operating conditions) and the volume occupied by the pipe in the soil. γ_b is the bulk unit weight of the soil. While ΔW has a minimal impact on lightweight pipes (such as pipes used in Wijewickreme et al. (2009) and this study), it can increase the normal force by up to 50% for heavy pipes used by Sheil et al. (2018).

Thirdly, f_R can be evaluated by the normalised roughness. As mentioned above, the critical normalised roughness among smooth, intermediate, and rough interfaces are 0.02 and 0.5, respectively (the framework of Paikowsky et al. (1995)). Experimental results by Paikowsky et al. (1995) and Lings & Dietz (2005) indicate that the interface friction angles increase linearly with the natural logarithm of the normalised roughness for intermediate interfaces and remain constant for smooth and rough interfaces. Therefore, f_R can be calculated as follows:

$$f_R = \begin{cases} \alpha + \beta \ln 0.02 & R_n \le 0.02 \\ \alpha + \beta \ln R_n & 0.02 < R_n < 0.5 \\ \alpha + \beta \ln 0.5 & R_n \ge 0.5 \end{cases} \tag{10}$$

where α and β are the empirical coefficients, whose values are dependent on the specific soil and interface in this study and affected by many other factors, such as void ratio, particle angularity, and grain size distribution. For the testing material in this study, α and β are taken as 1.13 and 0.20, respectively.

Substituting Eqs. (6) and (9) to (2), the new equation can be expressed as

$$T_{\max} = \pi D(\gamma' H \frac{1+K_0}{2} + 2G\frac{u_c}{D}\tan\psi_{\max} + \frac{D}{4}\Delta\gamma)\tan\left(f_R\varphi'\right) \tag{11}$$

Table 5 summarises the parameters for the new equation, incorporating data from Wijewickreme et al. (2009), Sheil et al. (2018) and the present study. Fig. 11 displays the newly predicted values based on these parameters. The Root Mean Square Error (RMSE) of the new model stands at 4.61, markedly lower than the 7.74 observed in the ALA predictions.

Conclusions

A new large-scale experimental system without boundary effects was developed to investigate the effects of surface roughness and coating hardness on the ASPI behaviour. The experimental setup involved testing five pipes with varying roughness and coating hardness in dense sand. Modified FSR sensors were used to measure the distribution and evolution of contact pressures on the soil-pipe interface and the earth pressures in the surrounding soils. Based on the experiments, the following conclusions were drawn:

The surface roughness significantly affects the pipe pullout resistance. The pullout resistance of the rough pipe is 1.70-1.85 times higher than that of the smooth pipe under the same buried condition. This increment is much greater than the value specified in current design guidelines (i.e., 0.17). Moreover, this increase stems from different mechanisms of roughness effects. The increase in interface friction coefficient accounts for 72-79%, while the remaining 21-28% is attributed to the contact pressure increase induced by the interrelated constrained dilation and soil arching.

Soil arching greatly affects the contact pressure between soil and pipes during both backfilling and pullout processes. During the backfilling, the contact pressures are concentrated at the shoulders and invert of the pipe due to the initial soil arching. During the pullout process, an additional soil arching due to the soil-interface dilation and a disturbance due to the loading determine contact pressure evolution behaviour. For the rough pipe, the former plays a dominant role. The thick shear band induces further relative displacement, leading to a noticeable increase in contact pressure at the pipe crown and invert. For the smooth pipe, the limited soil-interface dilation does not reinforce the soil arching. Instead, the pullout process disturbs the original equilibrium of the surrounding soil, releasing part of the internal friction of the initial soil arching. Consequently, the increase in contact pressure is only observed at the springlines of the smooth pipe.

For the test materials in this study, a critical coating hardness of approximately 35 HRA was identified based on experimental results. When the hardness is below this critical value (e.g., EA-coated pipes in this study), the pipes behave similarly to rough pipes due to an equivalent roughness caused by particle embedment. When the coating hardness exceeds this critical value (e.g., FBE-coated and raw steel pipes in this study), the influence of hardness seems limited.

A new method for predicting pullout resistance was proposed. This method considers the increase in normal force due to constrained dilatant and pipe weight, and it provides a quantitative estimation of the interface friction angle based on surface roughness. The new equation demonstrated good model capabilities, as verified using test results from previous studies and this study.

DATA AVAILABILITY STATEMENT

All data, models, and code generated or used during the study appear in the submitted article.

Acknowledgements

The authors would like to thank the Research Grants Council (RGC) of the HKSAR for providing financial support through grant N_PolyU526/23 and AoE/E-603/18. This work was also supported by RISUD/PolyU under Grant 1-BBWS.

NOTATION

$A(\gamma)$, $m(\gamma)$	strain-dependent parameters related to G
a_{ψ}, A_{ψ}, Q, R	empirical parameters related to $\psi_{\max}$
D	pipe outer diameter
d	distance from one end of the pipe test section
d_{50}	average particle size
$d\varepsilon_v$	volumetric strain increment
e, $e_{\max}$, e_{min}	void ratio, maximum void ratio and minimum void ratio
f, f_{R}	soil-pipe interface friction factor and roughness-dependent soil-pipe interface friction factor
G	soil shear modulus
H_{c}, H_{c0}	buried depth of the pipe crown and its real value in the experiment
I_{D}	relative density
K_0	coefficient of lateral earth pressure at rest
P	air pressure inside the flexible pneumatic bag
p_{a}	reference pressure of 100 kPa
$R_{\max}$, R_{a}	maximum height and average height deviations on the surface profile over a travel length of d_{50}
R_{n}	normalised surface roughness based on $R_{\max}$
S	thickness of the shear band
$T_{\max}$	pullout resistance, the maximum axial force per meter length
u, u_c	axial displacement and critical axial displacement
u_{r}	radial expanding displacement of the shear band due to interface dilation
α, β	empirical parameters related to f_{R}
γ, $d\gamma$	shear strain and shear strain increment
γ', γ_b, $\overline{\gamma}_{pipe}$, $\Delta\gamma$	soil effective unit weight, soil bulk unit weight, apparent unit weight of the pipe and unit weight difference between the pipe and soil
$\Delta\sigma_{\mathrm{D}}'$	the average increase in contact pressure caused by constrained dilation
ΔW	normal force increase per unit length caused by the pipe weight
δ, $\tan\delta$	soil-interface friction angle and soil-interface friction coefficient
μ_{ALA}, μ_{dir}	soil-pipe interface friction coefficient from the guidelines' prediction and interface direct shear tests
μ_{phy}	the ratio of the pullout resistance to the assumed contact force per unit length
σ_{c}'	nominal vertical pressure at the pipe crown
σ_i', σ_f'	initial effective stress and the effective stress at failure
φ'	sand internal friction angle
ψ, $\psi_{\max}$	dilation angle and maximum dilation angle

References

Abuel-Naga, H. M., Shaia, H. A. & Bouazza, A. (2018) Effect of Surface Roughness and Hardness of Continuum Materials on Interface Shear Strength of Granular Materials. *Journal of Testing and Evaluation* **46 (2)**: 826-831, https://doi.org/10.1520/JTE20160375.

Al-Khazaali, M. & Vanapalli, S. K. (2019) Axial force–displacement behaviour of a buried pipeline in saturated and unsaturated sand. *Géotechnique* **69 (11)**: 986-1003, https://doi.org/10.1680/jgeot.17.P.116.

ALA (American Lifeline Alliance) (2001) Guidelines for design of buried steel pipes. American Lifelines Alliance in Partnership with the Federal Emergency Management Agency (FEMA) and American Society for Civil Engineers (ASCE), Reston, VA, USA.

ASCE (American Society of Civil Engineers) (1984) Guidelines for the seismic design of oil and gas pipeline systems. Committee on Gas and Liquid Fuel Lifelines, American Society for Civil Engineering, New York, NY, USA.

ASTM (American Society for Testing Materials) (2022) ASTM E18: Standard Test Methods for Rockwell Hardness of Metallic Materials. ASTM International, West Conshohocken, PA, USA.

ASTM (American Society for Testing Materials) (2023) ASTM D785: Standard Test Method for Rockwell Hardness of Plastics and Electrical Insulating Materials. ASTM International, West Conshohocken, PA, USA.

Audibert, J. M. E. & Nyman, K. J. (1977) Soil Restraint Against Horizontal Motion of Pipes. *Journal of the Geotechnical Engineering Division* **103 (10)**: 1119-1142, https://doi.org/10.1061/AJGEB6.0000500.

Bolton, M. D. (1986) The strength and dilatancy of sands. *Geotechnique* **36 (1)**: 65-78, https://doi.org/10.1680/geot.1986.36.1.65.

BSI (British Standards Institution) (2002) BSI EN 10220:2002: Seamless and welded steel tubes. Dimensions and masses per unit length. BSI Group, London, UK.

CEDD (Civil Engineering and Development Department) (2020) General Specification for Civil Engineering Works (GS), Volume 2. Civil Engineering and Development Department, The Government of the Hong Kong Special Administrative Region, HK.

Chakraborty, T. & Salgado, R. (2010) Dilatancy and Shear Strength of Sand at Low Confining Pressures. *Journal of Geotechnical and Geoenvironmental Engineering* **136 (3)**: 527-532, https://doi.org/10.1061/(asce)gt.1943-5606.0000237.

Cui, S. Q., Zhou, C., Mu, Q. Y., *et al.* (2024) Coupled effects of temperature and suction on the shear behaviour of saturated and unsaturated clayey sand–structure interfaces. *Géotechnique*: 1-13, http://doi.org/10.1680/jgeot.22.00404.

DeJong, J. T. & Westgate, Z. J. (2009) Role of Initial State, Material Properties, and Confinement Condition on Local and Global Soil-Structure Interface Behavior. *Journal of Geotechnical and Geoenvironmental Engineering* **135 (11)**: 1646-1660, https://doi.org/10.1061/(ASCE)1090-0241(2009)135:11(1646).

Dove, J. E. & Frost, J. D. (1999) Peak Friction Behavior of Smooth Geomembrane-Particle Interfaces. *Journal of Geotechnical and Geoenvironmental Engineering* **125 (7)**: 544-555, http://doi.org/10.1061/(ASCE)1090-0241(1999)125:7(544).

Farhadi, B. & Lashkari, A. (2017) Influence of soil inherent anisotropy on behavior of crushed sand-steel interfaces. *Soils and Foundations* **57 (1)**: 111-125, https://doi.org/10.1016/j.sandf.2017.01.008.

Fretti, C., Lo Presti, D. C. F. & Pedroni, S. (1995) A Pluvial Deposition Method to Reconstitute Well-Graded Sand Specimens. *Geotechnical Testing Journal* **18 (2)**: 292-298, https://doi.org/10.1520/GTJ10330J.

Frost, J. D. & Han, J. (1999) Behavior of Interfaces between Fiber-Reinforced Polymers and Sands. *Journal of Geotechnical and Geoenvironmental Engineering* **125 (8)**: 633-640, http://doi.org/10.1061/(ASCE)1090-0241(1999)125:8(633).

Ghanadizadeh, A., Tabatabaie Shourijeh, P. & Lashkari, A. (2022) Laboratory investigation and constitutive modeling of the mechanical behavior of sand–GRP interfaces. *Acta Geotechnica* **17 (1)**: 1-23, https://doi.org/10.1007/s11440-022-01533-5.

Han, F., Ganju, E., Salgado, R., *et al.* (2018) Effects of Interface Roughness, Particle Geometry, and Gradation on the Sand–Steel Interface Friction Angle. *Journal of Geotechnical and Geoenvironmental Engineering* **144 (12)**: 04018096, https://doi.org/10.1061/(asce)gt.1943-5606.0001990.

HKIUS (Hong Kong Institute of Utility Specialists) (2011) Guide to utility management. Hong Kong Institute of Utility Specialists and Hong Kong Utility Research Centre, HK.

Houlsby, G. T. & Italiana, A. D. S. (1991) How the dilatancy of soils affects their behaviour In *Proceedings of the 10th European Conference on Soil Mechanics and Foundation Engineering*. Oxford, Firenze, Itália.

Interlink (2023) *FSR® Integration Guide & Evaluation Parts Catalog With Suggested Electrical Interfaces*. Interlink Electronics, Camarillo, Canada, See https://web.archive.org/web/20240315234554/http://www.tinyos.net.cn/datasheet/fsrguide.pdf (accessed 14/12/2023).

ISO (International Organization for Standardization) (2007) ISO 8501-1: Preparation of steel substrates before application of paints and related products — Visual assessment of surface cleanliness — Part 1: Rust grades and preparation grades of uncoated steel substrates and of steel substrates after overall removal of previous coatings. International Organization for Standardization ISO Central Secretariat, Vernier, Geneva, CH.

Kishida, H. & Uesugi, M. (1987) Tests of the interface between sand and steel in the simple shear apparatus. *Géotechnique* **37 (1)**: 45-52, https://doi.org/10.1680/geot.1987.37.1.45.

Klar, A. & Marshall, A. M. (2008) Shell versus beam representation of pipes in the evaluation of tunneling effects on pipelines. *Tunnelling and Underground Space Technology* **23 (4)**: 431-437, https://doi.org/10.1016/j.tust.2007.07.003.

Kootahi, K. & Leung, A. K. (2022) Effect of Soil Particle Size on the Accuracy of Tactile Pressure Sensors. *Journal of Geotechnical and Geoenvironmental Engineering* **148 (10)**: 06022008, https://doi.org/10.1061/(asce)gt.1943-5606.0002899.

Liang, H., Shen, Y., Xu, J. H., *et al.* (2021) Multiscale Three-Dimensional Morphological Characterization of Calcareous Sand Particles Using Spherical Harmonic Analysis. *Frontiers in Physics* **9 (1)**: 744319, http://doi.org/10.3389/fphy.2021.744319.

Lings, M. L. & Dietz, M. S. (2005) The Peak Strength of Sand-Steel Interfaces and the Role of Dilation. *Soils and Foundations* **45 (6)**: 1-14, https://doi.org/10.3208/sandf.45.1.

Liu, K. Y., Xu, C. S. & Zhang, X. L. (2021) Measurement Performance Evaluation of Tactile Pressure Sensor with Different Particle Sizes and Sensor Curvatures. *Geotechnical Testing Journal* **44 (4)**: 1036-1054, https://doi.org/10.1520/GTJ20200028.

Luo, S. Q., Tan, S. A. & Yong, K. Y. (2000) Pull-Out Resistance Mechanism of a Soil Nail Reinforcement in Dilative Soils. *Soils and Foundations* **40 (1)**: 47-56, https://doi.org/10.3208/sandf.40.47.

Marshall, A. M., Klar, A. & Mair, R. J. (2010) Tunneling beneath Buried Pipes: View of Soil Strain and Its Effect on Pipeline Behavior. *Journal of Geotechnical and Geoenvironmental Engineering* **136 (12)**: 1664-1672, http://doi.org/10.1061/(ASCE)GT.1943-5606.0000390.

Martinez, A. & Frost, J. D. (2017) The influence of surface roughness form on the strength of sand–structure interfaces. *Géotechnique Letters* **7 (1)**: 104-111, https://doi.org/10.1680/jgele.16.00169.

Meguid, M. A. (2019) Earth Pressure Distribution on Rigid Pipes Overlain by TDA Inclusion In *Proceedings of GeoMEast 2018*. Springer, Cairo, Egypt, pp. 1-13.

Meidani, M., Meguid, M. A. & Chouinard, L. E. (2017) Evaluation of Soil–Pipe Interaction under Relative Axial Ground Movement. *Journal of Pipeline Systems Engineering and Practice* **8 (4)**: 04017009, https://doi.org/10.1061/(asce)ps.1949-1204.0000269.

Ng, C. W. W., Zhou, C. & Chiu, C. F. (2020) Constitutive modelling of state-dependent behaviour of unsaturated soils: an overview. *Acta Geotechnica* **15 (10)**: 2705-2725, http://doi.org/10.1007/s11440-020-01014-7.

O'Rourke, T. D., Druschel, S. J. & Netravali, A. N. (1990) Shear Strength Characteristics of Sand - Polymer Interfaces. *Journal of Geotechnical Engineering* **116 (3)**: 451-469, https://doi.org/10.1061/(ASCE)0733-9410(1990)116:3(451).

Ooi, L. & Carter, J. (1987) A Constant Normal Stiffness Direct Shear Device for Static and Cyclic Loading. *Geotechnical Testing Journal* **10 (1)**: 3-12, http://doi.org/10.1520/GTJ10132J.

Oztoprak, S. & Bolton, M. D. (2013) Stiffness of sands through a laboratory test database. *Géotechnique* **63 (1)**: 54-70, http://doi.org/10.1680/geot.10.P.078.

Paikowsky, S., Player, C. M. & Connors, P. (1995) A Dual Interface Apparatus for Testing Unrestricted Friction of Soil Along Solid Surfaces. *Geotechnical Testing Journal* **18 (2)**: 168-193, https://doi.org/10.1520/GTJ10320J.

Pra-ai, S. & Boulon, M. (2016) Soil–structure cyclic direct shear tests: a new interpretation of the direct shear experiment and its application to a series of cyclic tests. *Acta Geotechnica* **12 (1)**: 107-127, https://doi.org/10.1007/s11440-016-0456-6.

PRCI (Pipeline Research Council International) (2009) Guidelines for constructing natural gas and liquid hydrocarbon pipelines. Design, Materials, and Construction Committee of Pipeline Research Council International, Inc, Chantilly, VA, USA.

Reza, A. & Dhar, A. S. (2021) Axial Pullout Behavior of Buried Medium-Density Polyethylene Gas Distribution Pipes. *International Journal of Geomechanics* **21 (7)**: 04021120, https://doi.org/10.1061/(ASCE)GM.1943-5622.0002101.

Scarpelli, G., Sakellariadi, E. & Furlani, G. (2003) Evaluation of soil-pipeline longitudinal interaction forces. *Rivista Italiana di Geotecnica* **4 (3)**: 24-41.

Sheil, B. B., Martin, C. M., Byrne, B. W., *et al.* (2018) Full-scale laboratory testing of a buried pipeline in sand subjected to cyclic axial displacements. *Géotechnique* **68 (8)**: 684-698, https://doi.org/10.1680/jgeot.16.P.275.

Trautmann, C. H. & O'Rourke, T. D. (1985) Lateral Force-Displacement Response of Buried Pipe. *Journal of Geotechnical Engineering* **111 (9)**: 1077-1092, http://doi.org/10.1061/(ASCE)0733-9410(1985)111:9(1077).

Trautmann, C. H., O'Rourke, T. D. & Kulhawy, F. H. (1985) Uplift Force-Displacement Response of Buried Pipe. *Journal of Geotechnical Engineering* **111 (9)**: 1061-1076, http://doi.org/10.1061/(ASCE)0733-9410(1985)111:9(1061).

USBR (United States Department of the Interior Bureau of Reclamation) (1996) USBR 1996: Geotechnical Training Manual No. 7: Pipe Bedding and Backfill. United States Department of the Interior Bureau of Reclamation, Technical Service Center Geotechnical Services, Denver, CO.

Wang, Y., Shi, J. W. & Ng, C. W. W. (2011) Numerical modeling of tunneling effect on buried pipelines. *Canadian Geotechnical Journal* **48 (7)**: 1125-1137, http://doi.org/10.1139/t11-024.

Wijewickreme, D., Karimian, H. & Honegger, D. (2009) Response of buried steel pipelines subjected to relative axial soil movement. *Canadian Geotechnical Journal* **46 (7)**: 735-752, https://doi.org/10.1139/t09-019.

Wijewickreme, D. & Weerasekara, L. (2015) Analytical Modeling of Field Axial Pullout Tests Performed on Buried Extensible Pipes. *International Journal of Geomechanics* **15 (2)**: 04014044, https://doi.org/10.1061/(ASCE)GM.1943-5622.0000388.

Yin, J. H., Hong, C. Y. & Zhou, W. H. (2012) Simplified Analytical Method for Calculating the Maximum Shear Stress of Nail-Soil Interface. *International Journal of Geomechanics* **12 (3)**: 309-317, https://doi.org/10.1061/(asce)gm.1943-5622.0000151.

Yin, J. H. & Su, L. J. (2006) An innovative laboratory box for testing nail pull-out resistance in soil. *Geotechnical Testing Journal* **29 (6)**: 451-461, https://doi.org/10.1520/GTJ100216.

Zhang, G., Wang, L. & Zhang, J. M. (2011) Dilatancy of the interface between a structure and gravelly soil. *Géotechnique* **61 (1)**: 75-84, https://doi.org/10.1680/geot.9.P.051.

Zhou, C., Tai, P. & Yin, J. H. (2020) A bounding surface model for saturated and unsaturated soil-structure interfaces. *International Journal for Numerical and Analytical Methods in Geomechanics* **44 (18)**: 2412-2429, https://doi.org/10.1002/nag.3123.

Table 1 Interface friction angle factor (ALA, 2001; PRCI, 2009)

Pipe Coating	f
Concrete	1.0
Coal tar	0.9
Rough steel	0.8
Smooth steel	0.7
Fusion-bonded epoxy	0.6
Polyethylene	0.6

Table 2 Sand and pipe properties

Soil Properties	
Specific gravity	2.68
Particle size: mm	0.25-0.5
Median particle size, d_{50}: mm	0.375
Maximum void ratio, $e_{\max}$	0.797
Minimum void ratio, $e_{\min}$	0.526
Target relative density, I_D: %	85
Dry unit weight at target relative density, γ': kN/m^3	17.0
Peak friction angle*: °	39.6
Critical state friction angle*: °	32.8
Particle spericity†	0.92
Particle roundness†	0.728
Particle roughness†	1.021
Pipe Properties	
Diameter, D: mm	102
Thickness: mm	4
Total length: m	1.25
Testing length: m	0.7
Steel density: kg/m^3	7930
Young's modulus: MPa	204
Poisson's ratio	0.3

*Measured by direct shear tests with applied effective normal stresses of 17, 34, 50, and 100 kPa.
†Data from Liang et al. (2021).

Table 3 Pipe surface conditions and soil-pipe interface properties

Pipe type	Surface treatment	R_{max}: mm	R_n*	R_a: mm	Surface material hardness: HRA†	Peak friction angle‡: °	Critical state friction angle‡: °
Smooth	Raw seamless steel pipe	0.015	0.04	0.0024	59.0	18.4	17.3
Intermediate	Turning surface	0.08	0.21	0.0313	59.0	34.7	29.4
Rough	Turning surface	0.38	1.01	0.0944	59.0	37.9	33.5
FBE	Fusion bonded epoxy coated	0.004	0.01	0.0006	44.3	19.2	19.0
EA	Epoxy asphalt coated	0.003	0.01	0.0004	32.6	36.8	33.8

*R_n: Normalised surface roughness using R_{max}/d_{50}.

†HRA: Rockwell hardness based on ASTM E18 and ASTM D785.

‡Measured by interface direct shear tests with applied effective normal stresses of 17, 34, 50, and 100 kPa.

Table 4. Testing program

	Reference	Roughness or coating	Nominal pressure at the pipe crown: kPa
Series I Roughness and stress effects	Smooth-17	Smooth steel	17
	Smooth-34	Smooth steel	34
	Smooth-50	Smooth steel	50
	Rough-17	Rough steel	17
	Rough-34	Rough steel	34
	Rough-50	Rough steel	50
	Intermediate-34	Intermediate steel	34
Series II Coating hardness effects	Smooth-34	Smooth steel	34
	EA-34	EA-coated steel	34
	FBE-34	FBE-coated steel	34

Table 5. Parameters for new equation verification

Parameters	This study					Wijewickreme et al. (2009)		Sheil, B. B. et al. (2018)
	Smooth	Intermediate	Rough	FBE	EA	AB-3, 4, 6	AB-5	H1-4
Pipe diameter, D: mm	102	102	102	102	102	457	457	350
Normalised roughness, R_n	0.04	0.21	1.01	0.01	0.01	0.84	0.84	0.11
Parameter, α	1.13	1.13	1.13	-	-	-	-	-
Parameter, β	0.2	0.2	0.2	-	-	-	-	-
Interface friction factor, f	Eq. (10)	Eq. (10)	Eq. (10)	0.49	0.93	0.81	0.74	0.79
Unit weight difference, $\Delta\gamma$: kN/m^3	4.53	4.53	4.53	4.53	4.53	2.43	2.43	27.34
Nominal pressure at the pipe crown, σ_c': kPa	17-50	34	17-50	34	34	17.91	17.53	6.9-50
Internal friction angle, φ': °	39.6	39.6	39.6	39.6	39.6	44.5	44.5	37.9
Relative density, I_D: %	85	85	85	85	85	75	20	12
Void ratio, e	0.57	0.57	0.57	0.57	0.57	0.7	0.88	0.94
$A(\gamma)$	126	126	126	126	126	126	126	126
$m(\gamma)$	1	1	1	1	1	1	1	1
Critical displacement, u_c: mm	0.77	1.7	2.85	1.85	3.76	2.6	-	-

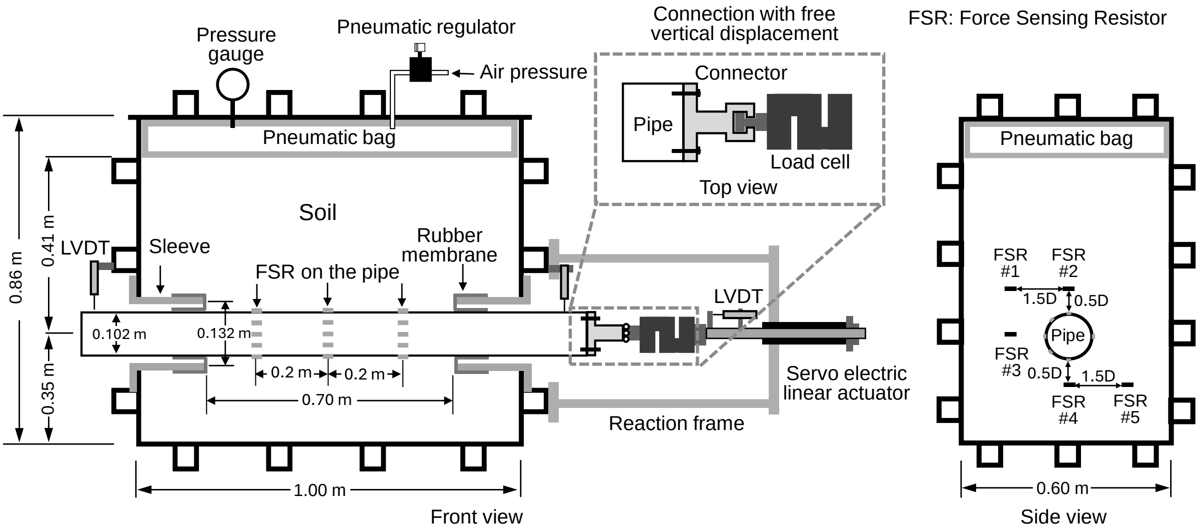

Fig. 1. Schematic diagram of the experimental system

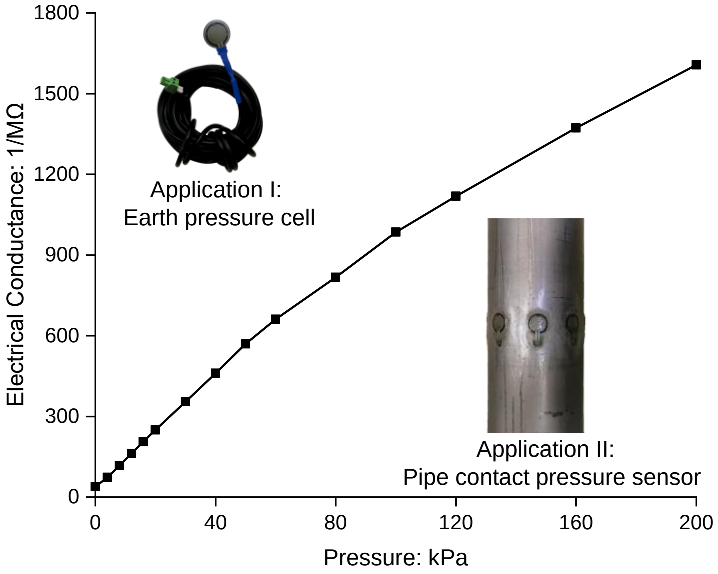

Fig. 2. Typical calibrated electrical conductance-pressure relationship of FSR sensors

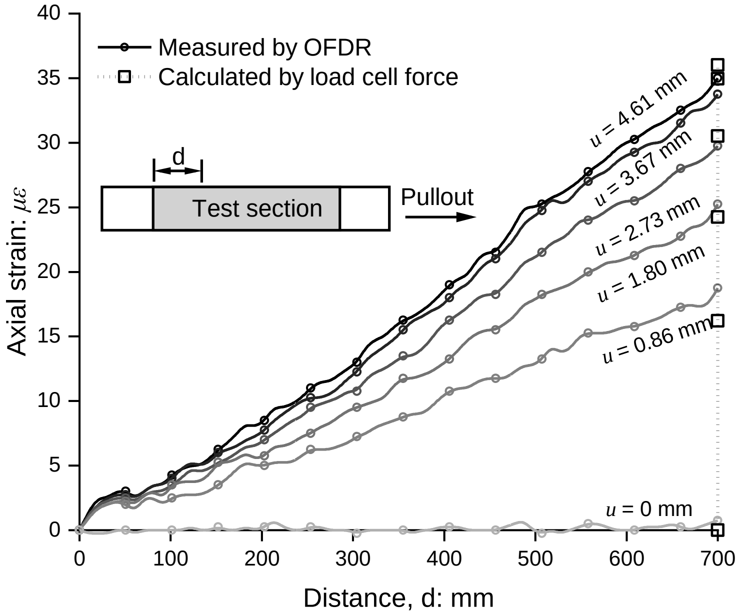

Fig. 3. Axial strain distribution in Rough-50 measured by OFDR (optical frequency domain reflectometry) with different axial displacements (*u*)

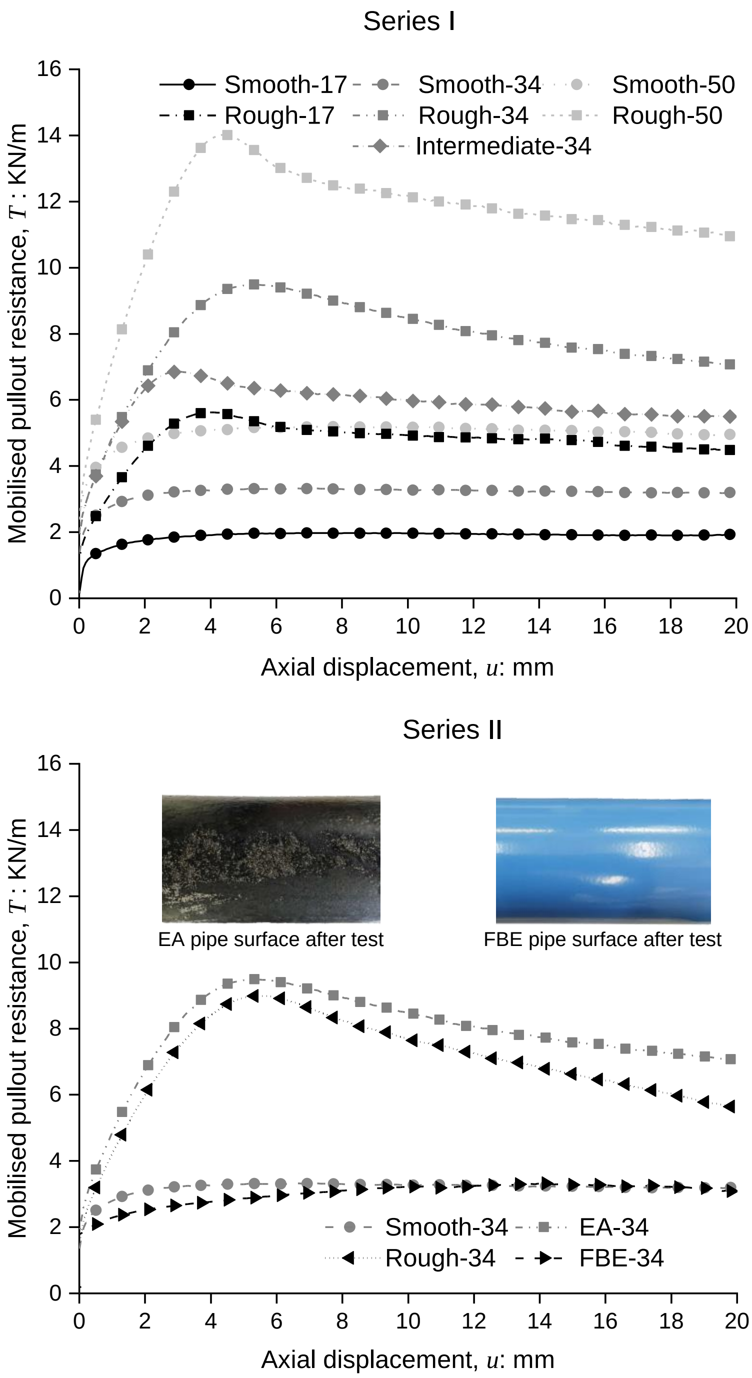

Fig. 4. Axial force-displacement relationship

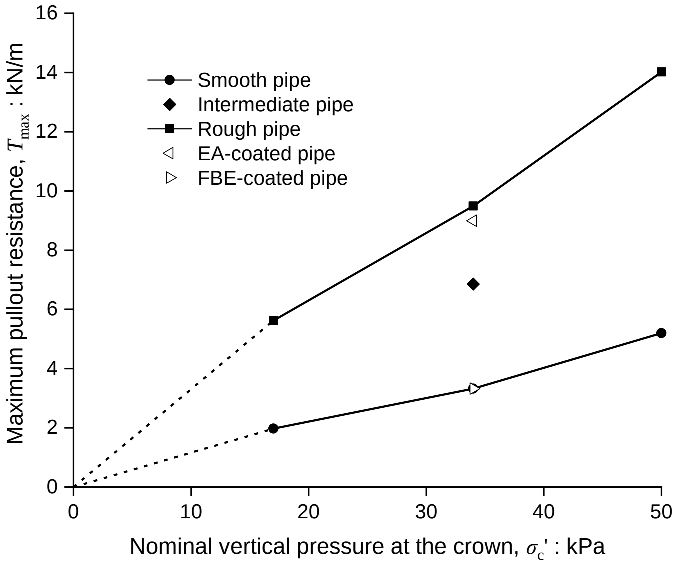

Fig. 5. Nominal vertical pressure at the crown against the pullout resistance

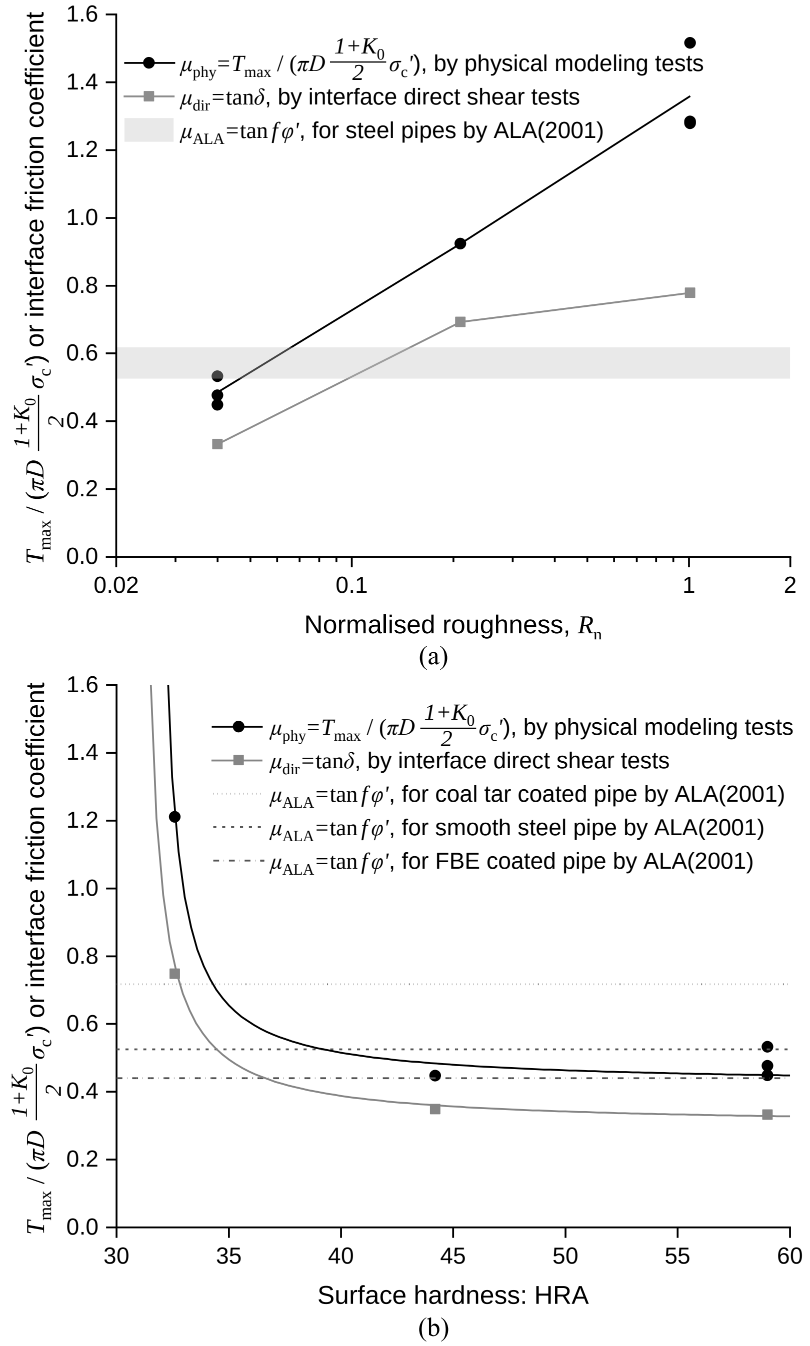

Fig. 6. Comparison between μ_{phy} and interface friction coefficient: (a) normalised roughness; (b) surface hardness

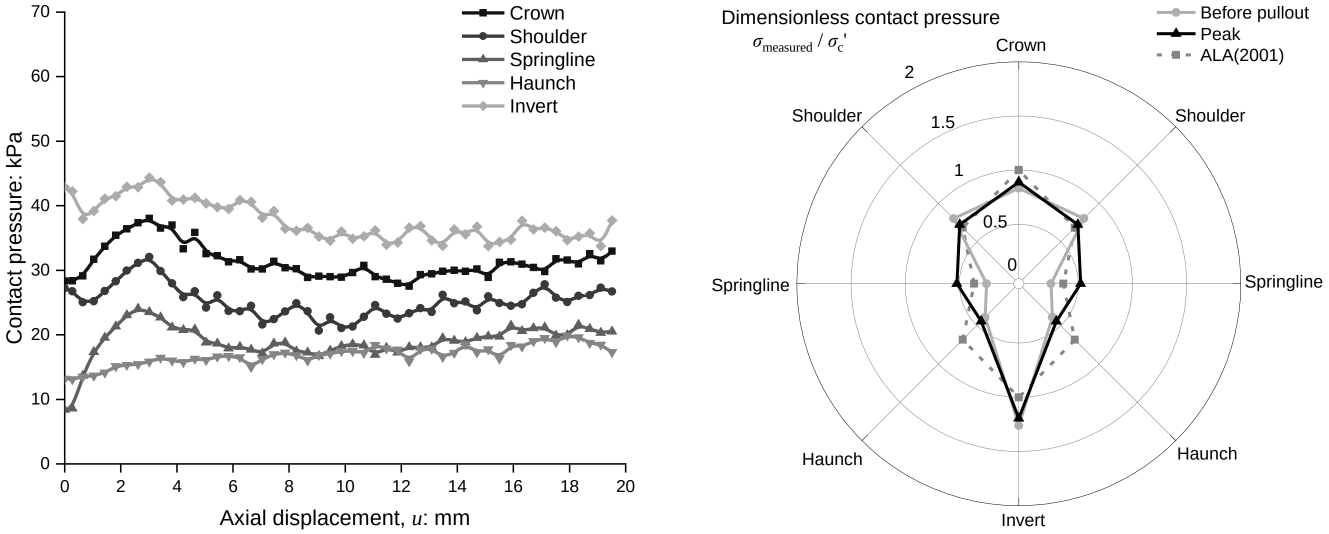

(a)

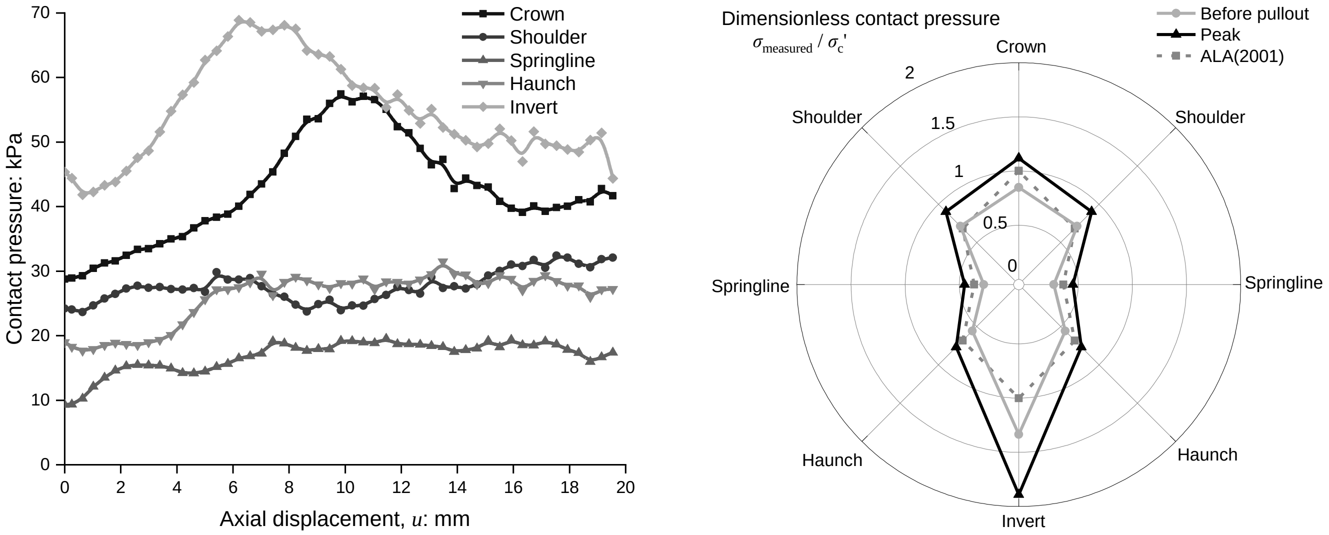

(b)

Fig. 7. Contact pressure development and distribution: (a) Smooth-34; (b) Rough-34

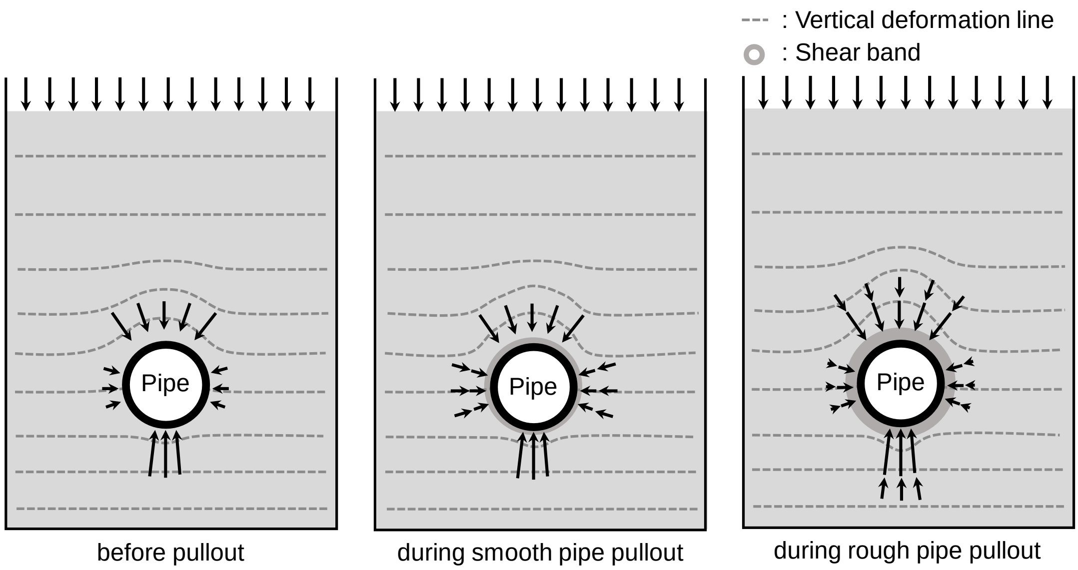

Fig. 8. Schematic diagram of soil arching effect on pipes

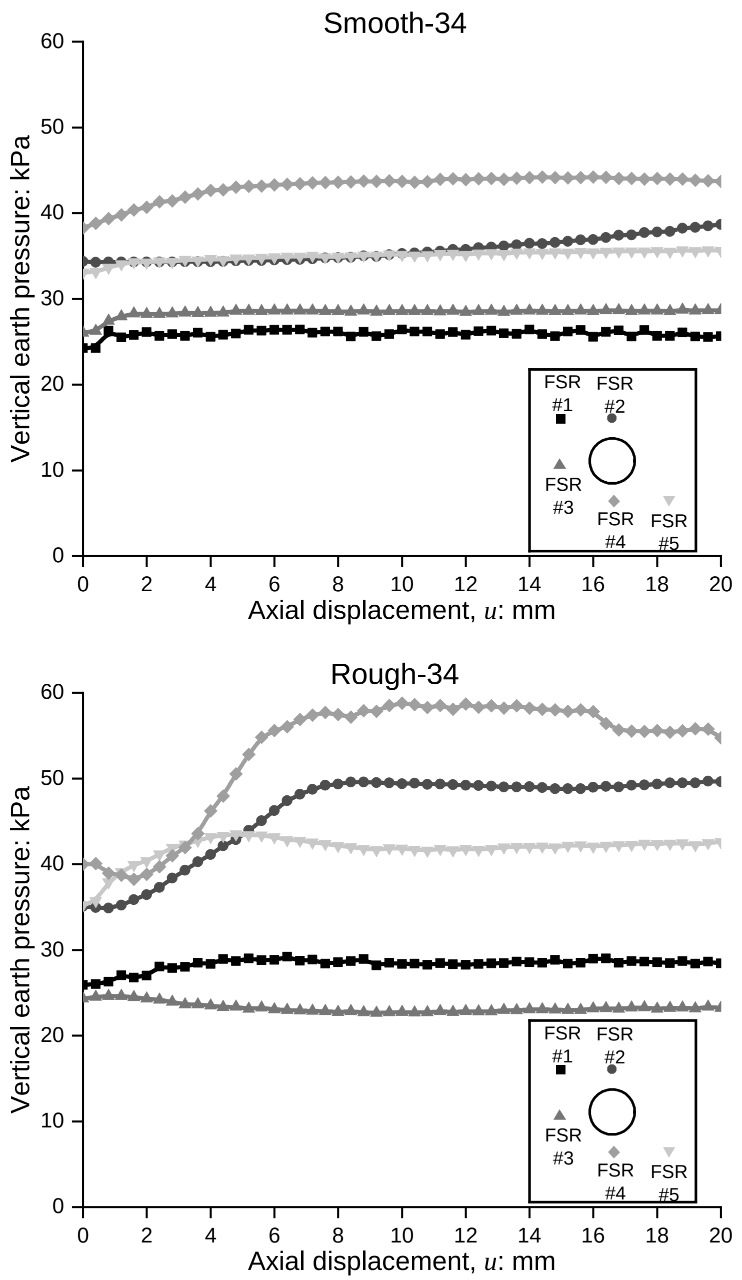

Fig. 9. Vertical earth pressure development

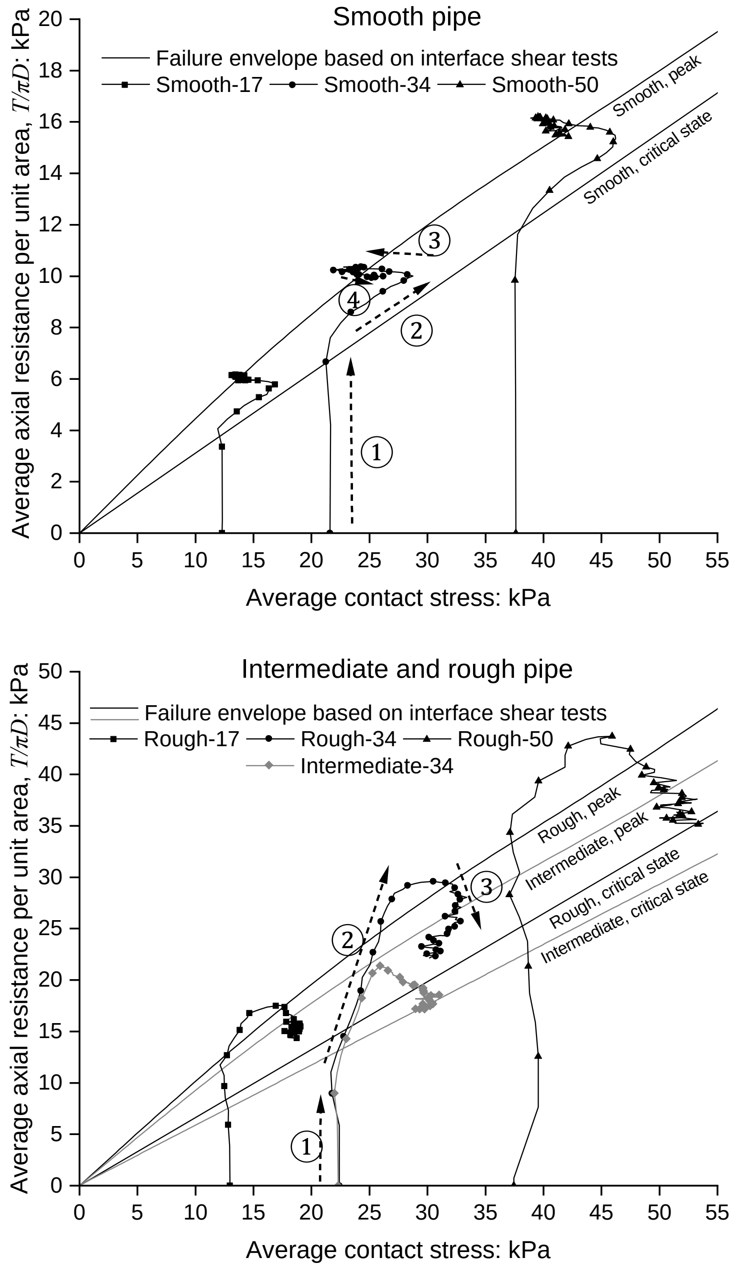

Fig. 10. Stress path based on average contact pressure measured by FSR

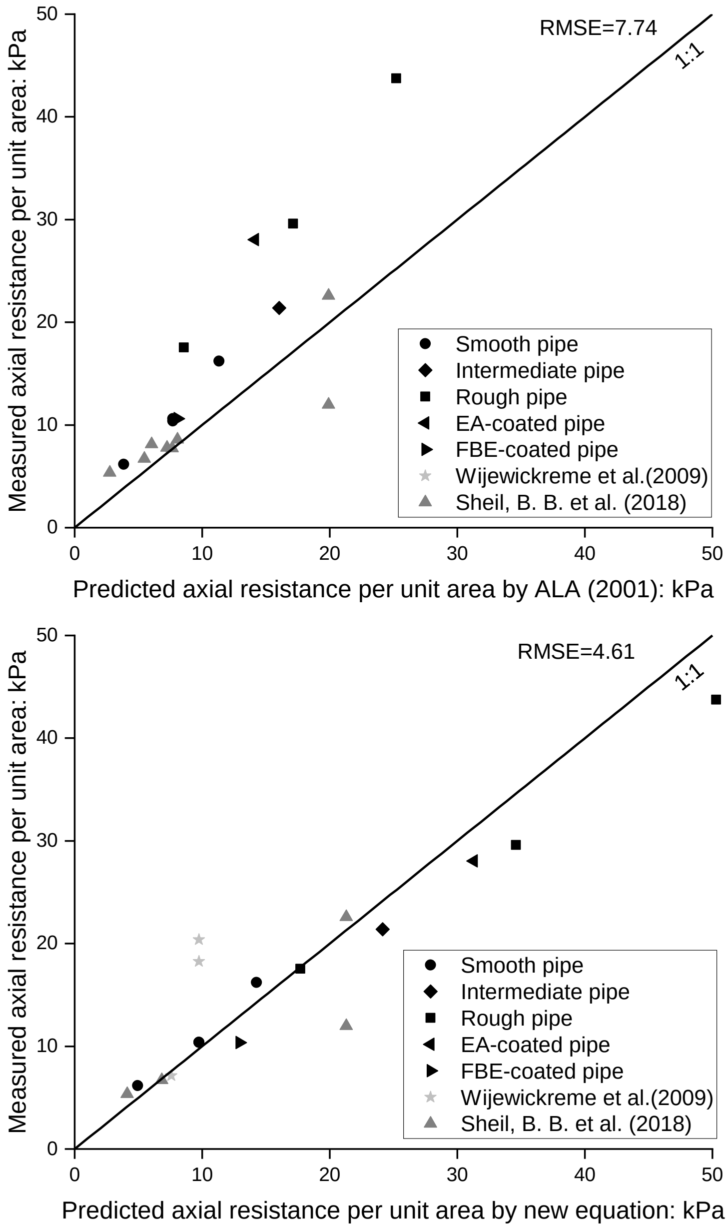

Fig. 11. Prediction of pullout resistance